Electronic Supplementary Material (ESI) for CrystEngComm.

Prediction of CO_2 Adsorption Properties of Azo, Azoxy and Azodioxy-linked Porous Organic Polymers Guided by Electrostatic Potential

Tea Frey, Barbara Panić, Petar Šutalo, Mladen Borovina, Ivana Biljan* and Ivan Kodrin*

Supporting information

Table of Contents

1. Interactions of CO_2 and N_2 with the selected organic molecules/fragments

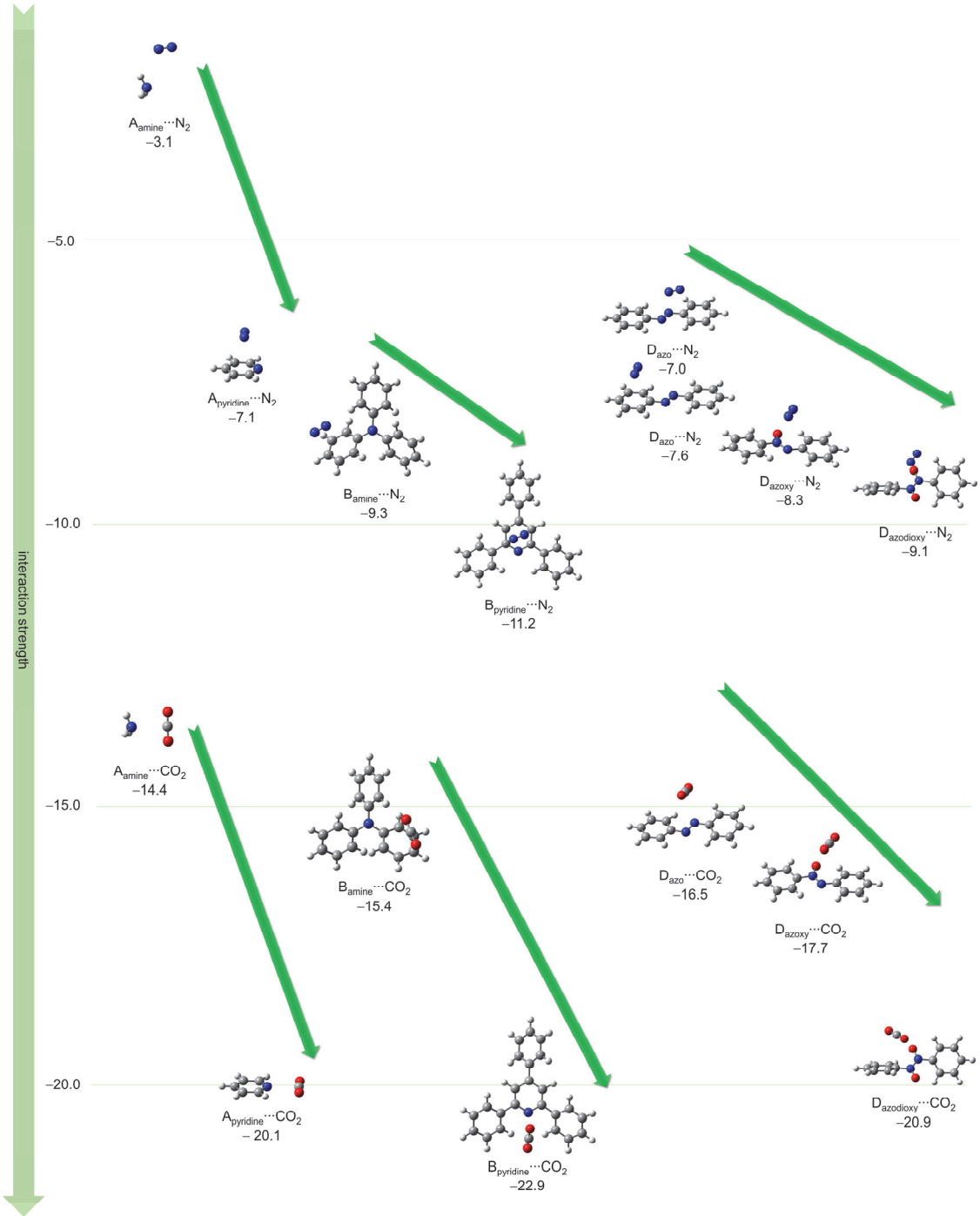

Figure S1. The B3LYP-D3(BJ)/def2-TZVP optimized geometries of the most stable complexes of fragments **A** and **B** (amine vs. pyridine) and fragments **D** (azo vs. azoxy vs. azodioxy, modeled in our previous study) with one molecule of N_2 or CO_2. The calculated BSSE corrected interaction energies (E_{int} in kJ mol^{-1}) are shown under the structures. The green arrows indicate interactions that become stronger after structural changes.

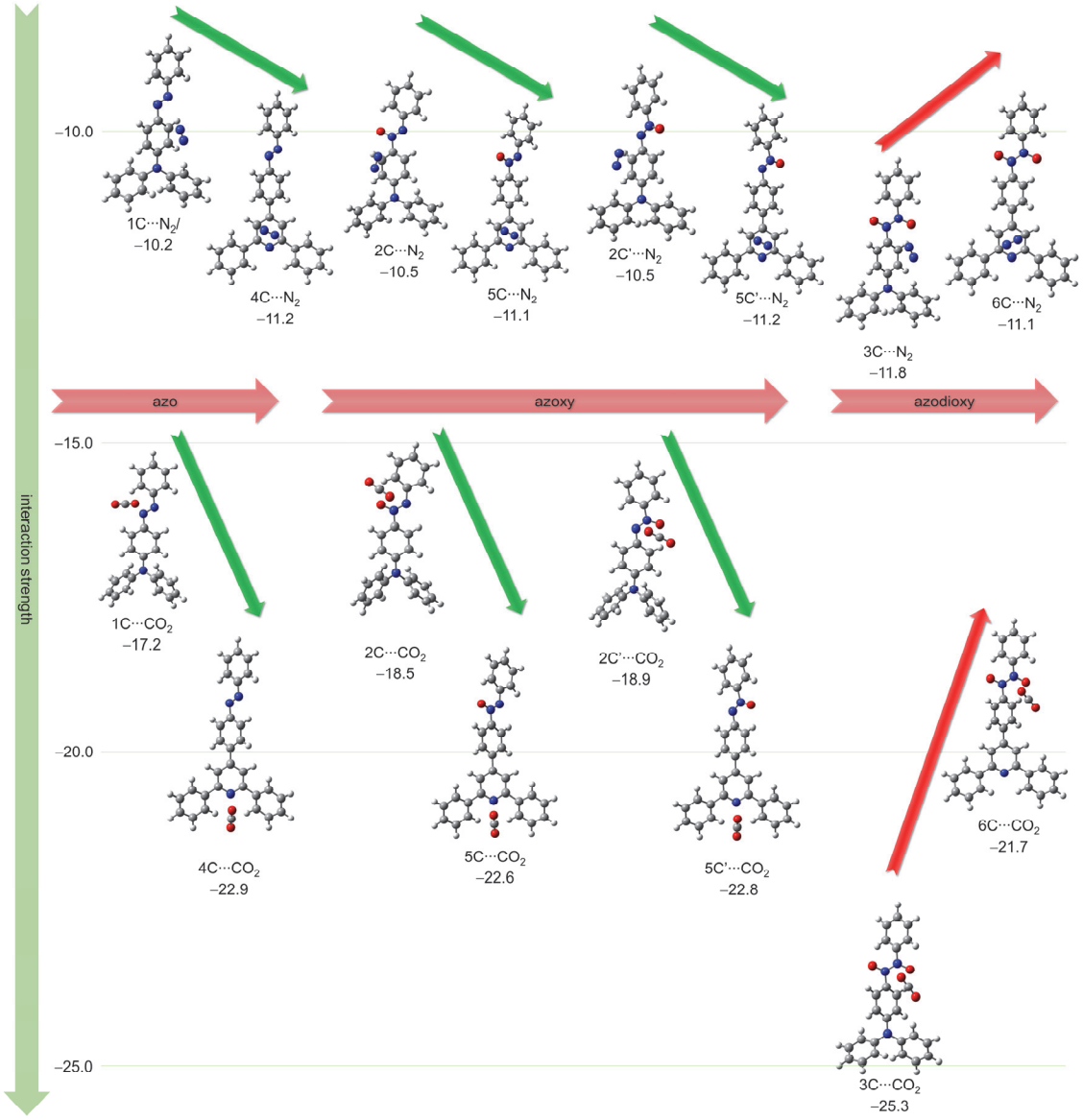

Figure S2. The B3LYP-D3(BJ)/def2-TZVP optimized geometries of the most stable complexes of fragment **C** (TPA and TPP trigonal building units connected to phenyl ring by azo, azoxy or azodioxy bond) with one molecule of N_2 or CO_2. The calculated BSSE corrected interaction energies (E_{int} in kJ mol^{-1}) are shown under the structures. The green arrows indicate interactions that become stronger after structural changes. The red arrows indicate interactions that become weaker after the structural changes. Oxygen in azoxy bond adopts two orientations, one in which it is closer to the trigonal building unit (2C and 5C), and the other in which it is closer to the upper phenyl ring (2C' and 5C').

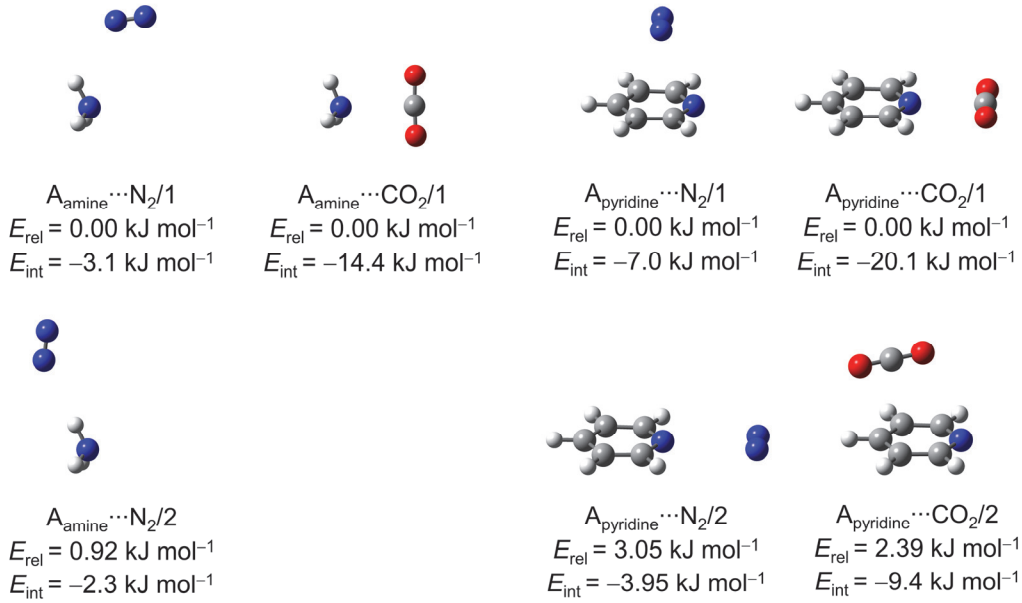

Figure S3. The B3LYP-D3(BJ)/def2-TZVP optimized geometries of the selected complexes between fragments **A_{amine}** and **$A_{pyridine}$** and one molecule of N_2 or CO_2. Relative energies of the selected complexes (E_{rel}) and BSSE corrected interaction energies (E_{int}).

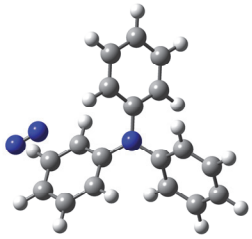

Figure S4. The B3LYP-D3(BJ)/def2-TZVP optimized geometries of the selected complexes between fragment **B_{amine}** and one molecule of N_2. Relative energies of the selected complexes (E_{rel}) and BSSE corrected interaction energies (E_{int}).

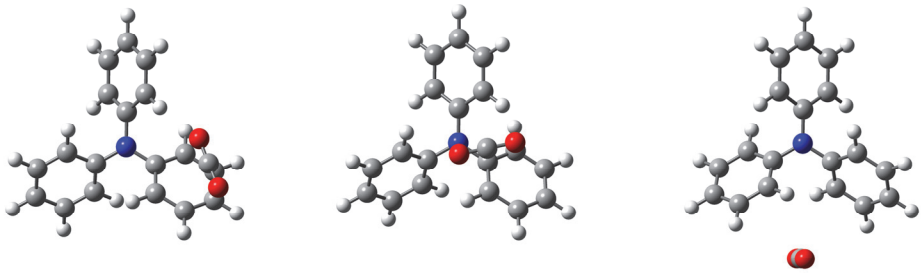

$B_{amine}\cdots CO_2/1$
E_{rel} = 0.00 kJ mol^{-1}
E_{int} = –15.4 kJ mol^{-1}

$B_{amine}\cdots CO_2/2$
E_{rel} = 0.02 kJ mol^{-1}
E_{int} = –15.8 kJ mol^{-1}

$B_{amine}\cdots CO_2/3$
E_{rel} = 0.04 kJ mol^{-1}
E_{int} = –15.4 kJ mol^{-1}

Figure S5. The B3LYP-D3(BJ)/def2-TZVP optimized geometries of the selected complexes between fragment $\mathbf{B_{amine}}$ and one molecule of CO_2. Relative energies of the selected complexes (E_{rel}) and BSSE corrected interaction energies (E_{int}).

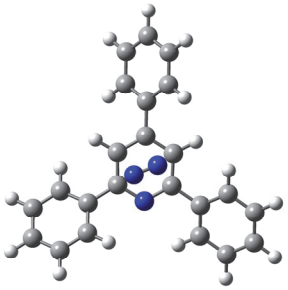

$B_{pyridine}\cdots N_2/1$
E_{rel} = 0.00 kJ mol^{-1}
E_{int} = –11.2 kJ mol^{-1}

Figure S6. The B3LYP-D3(BJ)/def2-TZVP optimized geometries of the selected complexes between fragment $\mathbf{B_{pyridine}}$ and one molecule of N_2. Relative energies of the selected complexes (E_{rel}) and BSSE corrected interaction energies (E_{int}).

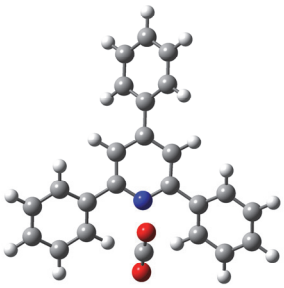

$B_{pyridine}\cdots CO_2/1$
E_{rel} = 0.00 kJ mol^{-1}
E_{int} = –22.9 kJ mol^{-1}

Figure S7. The B3LYP-D3(BJ)/def2-TZVP optimized geometries of the selected complexes between fragment **$B_{pyridine}$** and one molecule of CO_2. Relative energies of the selected complexes (E_{rel}) and BSSE corrected interaction energies (E_{int}).

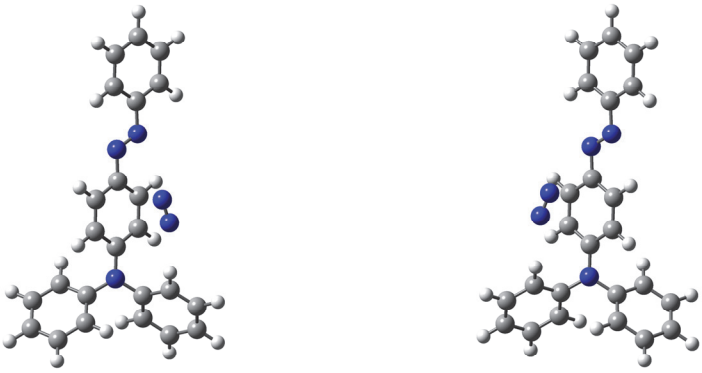

1C$\cdots N_2/1$
E_{rel} = 0.00 kJ mol^{-1}
E_{int} = –10.2 kJ mol^{-1}

1C$\cdots N_2/2$
E_{rel} = 0.00 kJ mol^{-1}
E_{int} = –10.2 kJ mol^{-1}

Figure S8. The B3LYP-D3(BJ)/def2-TZVP optimized geometries of the selected complexes between fragment **1C** and one molecule of N_2. Relative energies of the selected complexes (E_{rel}) and BSSE corrected interaction energies (E_{int}).

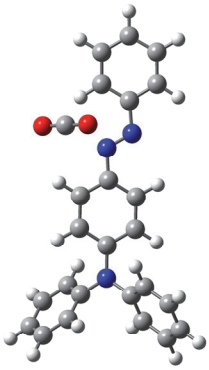

1C···CO_2/1
E_{rel} = 0.00 kJ mol^{-1}
E_{int} = –17.2 kJ mol^{-1}

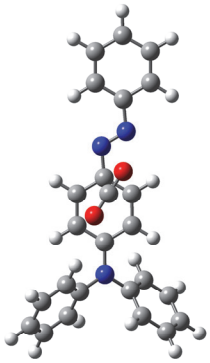

1C···CO_2/2
E_{rel} = 0.09 kJ mol^{-1}
E_{int} = –16.3 kJ mol^{-1}

Figure S9. The B3LYP-D3(BJ)/def2-TZVP optimized geometries of the selected complexes between fragment **1C** and one molecule of CO_2. Relative energies of the selected complexes (E_{rel}) and BSSE corrected interaction energies (E_{int}).

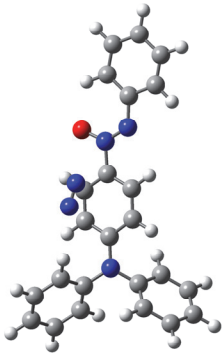

2C···N_2/1
E_{rel} = 0.00 kJ mol^{-1}
E_{int} = –10.5 kJ mol^{-1}

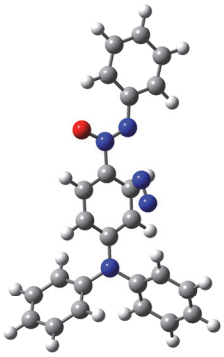

2C···N_2/2
E_{rel} = 0.00 kJ mol^{-1}
E_{int} = –10.5 kJ mol^{-1}

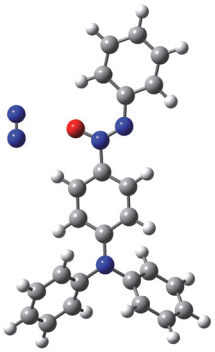

2C···N_2/3
E_{rel} = 5.01 kJ mol^{-1}
E_{int} = –5.6 kJ mol^{-1}

Figure S10. The B3LYP-D3(BJ)/def2-TZVP optimized geometries of the selected complexes between fragment **2C** and one molecule of N_2. Relative energies of the selected complexes (E_{rel}) and BSSE corrected interaction energies (E_{int}).

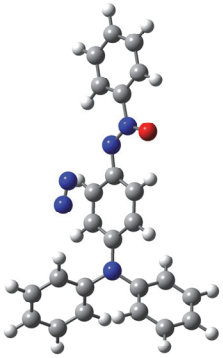

2C' ···N_2/1
E_{rel} = 0.00 kJ mol^{-1}
E_{int} = –10.5 kJ mol^{-1}

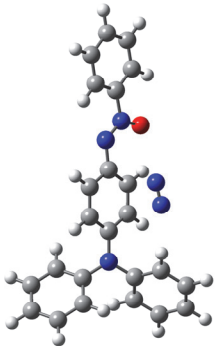

2C' ···N_2/2
E_{rel} = 0.03 kJ mol^{-1}
E_{int} = –10.5 kJ mol^{-1}

Figure S11. The B3LYP-D3(BJ)/def2-TZVP optimized geometries of the selected complexes between fragment **2C'** and one molecule of N_2. Relative energies of the selected complexes (E_{rel}) and BSSE corrected interaction energies (E_{int}).

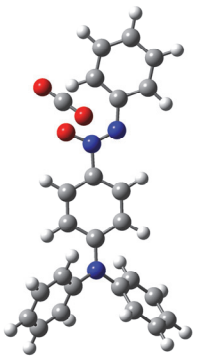

2C···CO_2/1
E_{rel} = 0.00 kJ mol^{-1}
E_{int} = –18.5 kJ mol^{-1}

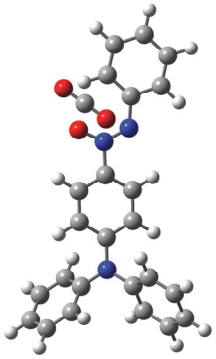

2C···CO_2/2
E_{rel} = 0.05 kJ mol^{-1}
E_{int} = –18.4 kJ mol^{-1}

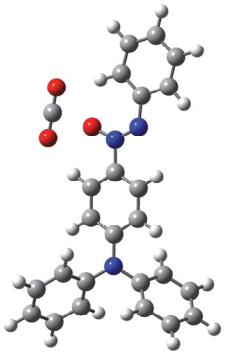

2C···CO_2/3
E_{rel} = 2.98 kJ mol^{-1}
E_{int} = –15.6 kJ mol^{-1}

Figure S12. The B3LYP-D3(BJ)/def2-TZVP optimized geometries of the selected complexes between fragment **2C** and one molecule of CO_2. Relative energies of the selected complexes (E_{rel}) and BSSE corrected interaction energies (E_{int}).

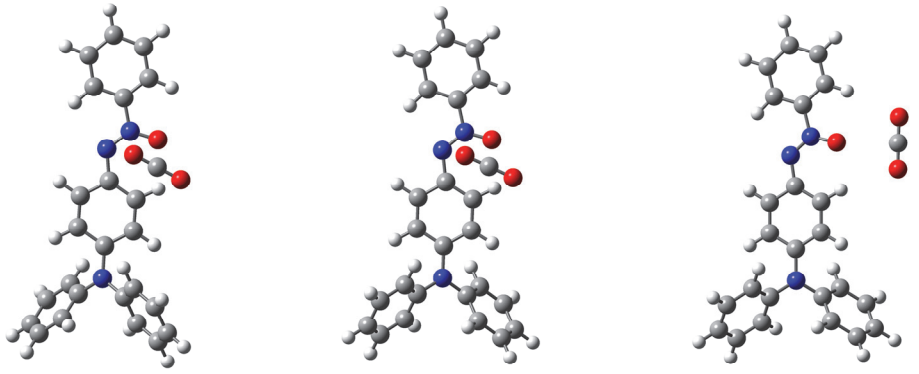

2C' ···N_2/1
E_{rel} = 0.00 kJ mol^{-1}
E_{int} = –18.9 kJ mol^{-1}

2C' ···N_2/2
E_{rel} = 0.06 kJ mol^{-1}
E_{int} = –18.7 kJ mol^{-1}

2C' ···N_2/3
E_{rel} = 2.96 kJ mol^{-1}
E_{int} = –16.0 kJ mol^{-1}

Figure S13. The B3LYP-D3(BJ)/def2-TZVP optimized geometries of the selected complexes between fragment **2C'** and one molecule of CO_2. Relative energies of the selected complexes (E_{rel}) and BSSE corrected interaction energies (E_{int}).

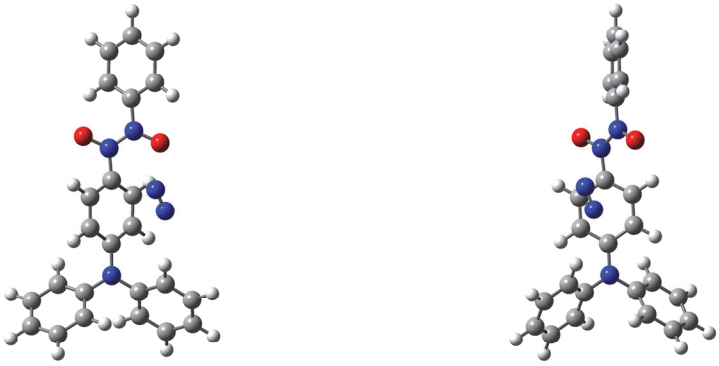

3C···N_2/1
E_{rel} = 0.00 kJ mol^{-1}
E_{int} = –11.8 kJ mol^{-1}

3C···N_2/2
E_{rel} = 0.04 kJ mol^{-1}
E_{int} = –11.3 kJ mol^{-1}

Figure S14. The B3LYP-D3(BJ)/def2-TZVP optimized geometries of the selected complexes between fragment **3C** and one molecule of N_2. Relative energies of the selected complexes (E_{rel}) and BSSE corrected interaction energies (E_{int}).

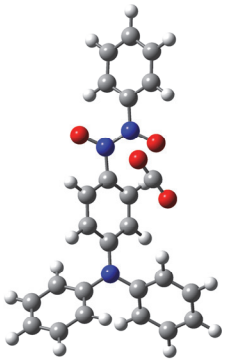

3C···CO_2/1
E_{rel} = 0.00 kJ mol^{-1}
E_{int} = –25.3 kJ mol^{-1}

Figure S15. The B3LYP-D3(BJ)/def2-TZVP optimized geometries of the selected complexes between fragment **3C** and one molecule of CO_2. Relative energies of the selected complexes (E_{rel}) and BSSE corrected interaction energies (E_{int}).

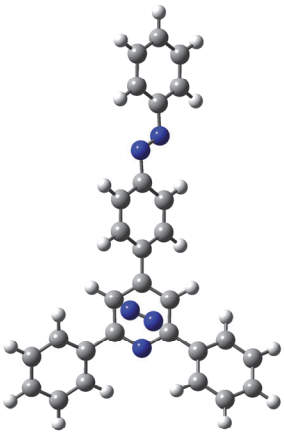

4C···N_2/1
E_{rel} = 0.00 kJ mol^{-1}
E_{int} = –11.2 kJ mol^{-1}

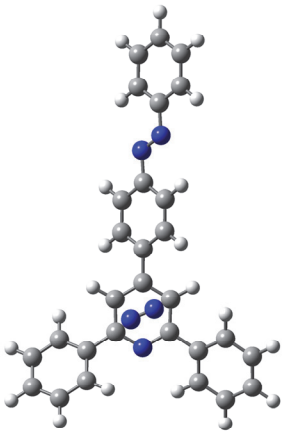

4C···N_2/2
E_{rel} = 0.01 kJ mol^{-1}
E_{int} = –11.2 kJ mol^{-1}

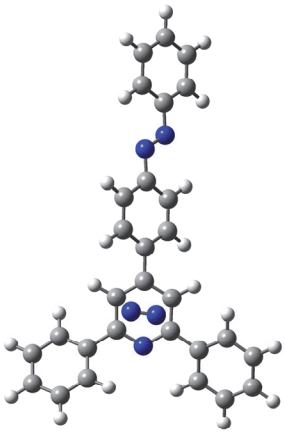

4C···N_2/3
E_{rel} = 0.15 kJ mol^{-1}
E_{int} = –11.0 kJ mol^{-1}

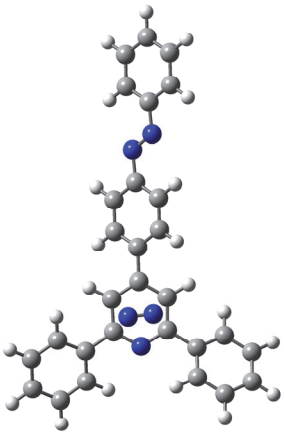

4C···N_2/4
E_{rel} = 0.15 kJ mol^{-1}
E_{int} = –10.9 kJ mol^{-1}

Figure S16. The B3LYP-D3(BJ)/def2-TZVP optimized geometries of the selected complexes between fragment **4C** and one molecule of N_2. Relative energies of the selected complexes (E_{rel}) and BSSE corrected interaction energies (E_{int}).

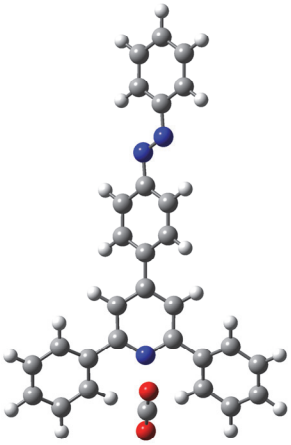

4C···CO_2/1
E_{rel} = 0.00 kJ mol^{-1}
E_{int} = –22.9 kJ mol^{-1}

Figure S17. The B3LYP-D3(BJ)/def2-TZVP optimized geometries of the selected complexes between fragment **4C** and one molecule of CO_2. Relative energies of the selected complexes (E_{rel}) and BSSE corrected interaction energies (E_{int}).

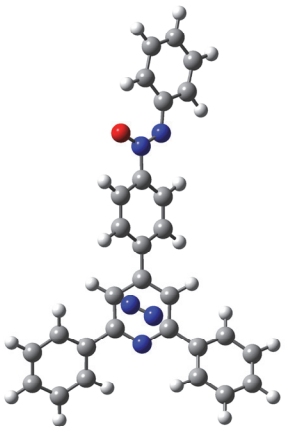

5C···N_2/1
E_{rel} = 0.00 kJ mol^{-1}
E_{int} = –11.1 kJ mol^{-1}

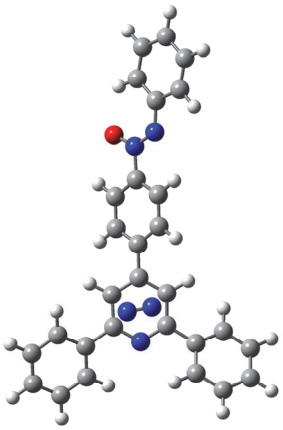

5C···N_2/2
E_{rel} = 0.09 kJ mol^{-1}
E_{int} = –10.9 kJ mol^{-1}

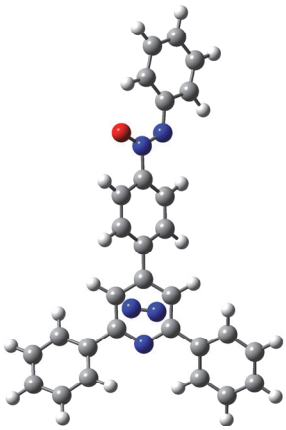

5C···N_2/3
E_{rel} = 0.09 kJ mol^{-1}
E_{int} = –10.9 kJ mol^{-1}

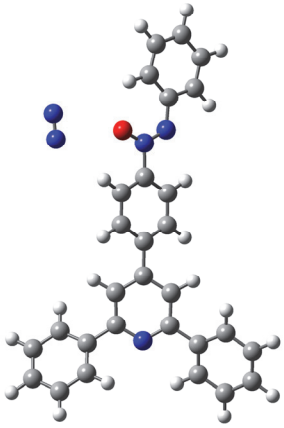

5C···N_2/4
E_{rel} = 5.68 kJ mol^{-1}
E_{int} = –5.6 kJ mol^{-1}

Figure S18. The B3LYP-D3(BJ)/def2-TZVP optimized geometries of the selected complexes between fragment **5C** and one molecule of N_2. Relative energies of the selected complexes (E_{rel}) and BSSE corrected interaction energies (E_{int}).

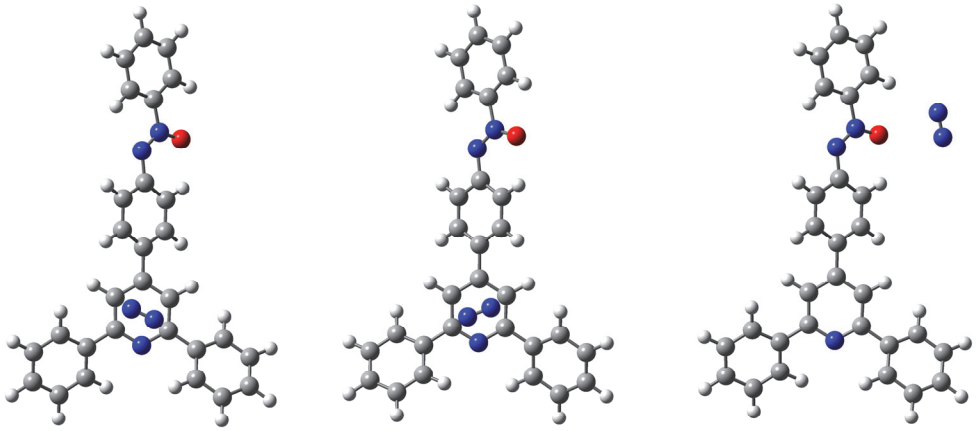

5C'···N_2/1
E_{rel} = 0.00 kJ mol^{-1}
E_{int} = –11.2 kJ mol^{-1}

5C'···N_2/2
E_{rel} = 0.03 kJ mol^{-1}
E_{int} = –11.1 kJ mol^{-1}

5C'···N_2/3
E_{rel} = 5.87 kJ mol^{-1}
E_{int} = –5.5 kJ mol^{-1}

Figure S19. The B3LYP-D3(BJ)/def2-TZVP optimized geometries of the selected complexes between fragment **5C'** and one molecule of N_2. Relative energies of the selected complexes (E_{rel}) and BSSE corrected interaction energies (E_{int}).

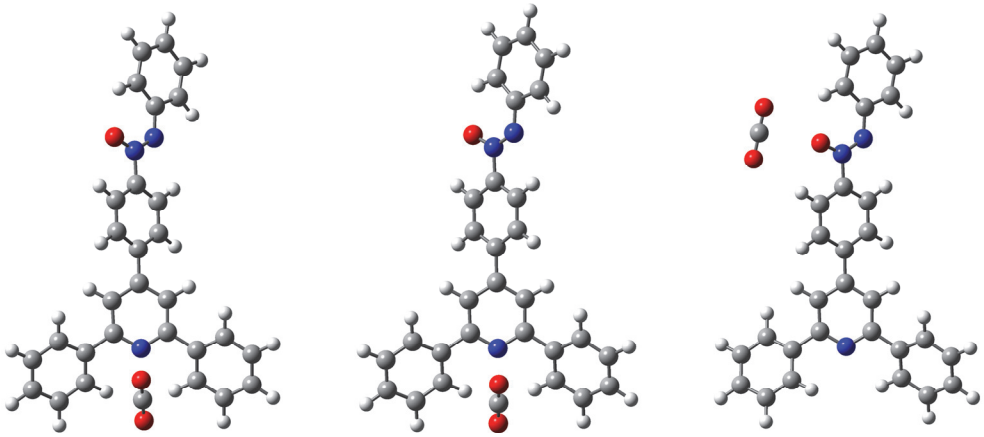

5C···CO_2/1
E_{rel} = 0.00 kJ mol^{-1}
E_{int} = –22.6 kJ mol^{-1}

5C···CO_2/2
E_{rel} = 0.03 kJ mol^{-1}
E_{int} = –22.6 kJ mol^{-1}

5C···CO_2/3
E_{rel} = 6.30 kJ mol^{-1}
E_{int} = –15.2 kJ mol^{-1}

Figure S20. The B3LYP-D3(BJ)/def2-TZVP optimized geometries of the selected complexes between fragment **5C** and one molecule of CO_2. Relative energies of the selected complexes (E_{rel}) and BSSE corrected interaction energies (E_{int}).

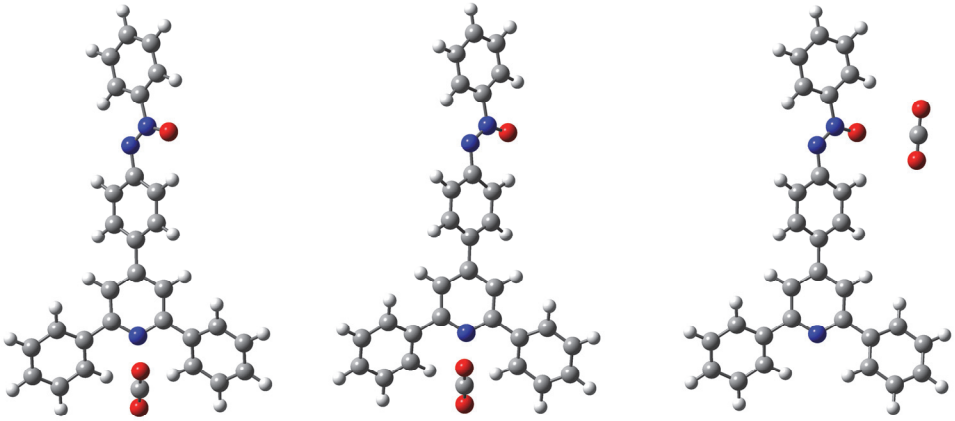

5C'···CO_2/1
E_{rel} = 0.00 kJ mol^{-1}
E_{int} = –22.8 kJ mol^{-1}

5C'···CO_2/2
E_{rel} = 0.05 kJ mol^{-1}
E_{int} = –22.8 kJ mol^{-1}

5C'···CO_2/3
E_{rel} = 6.50 kJ mol^{-1}
E_{int} = –15.3 kJ mol^{-1}

Figure S21. The B3LYP-D3(BJ)/def2-TZVP optimized geometries of the selected complexes between fragment **5C'** and one molecule of CO_2. Relative energies of the selected complexes (E_{rel}) and BSSE corrected interaction energies (E_{int}).

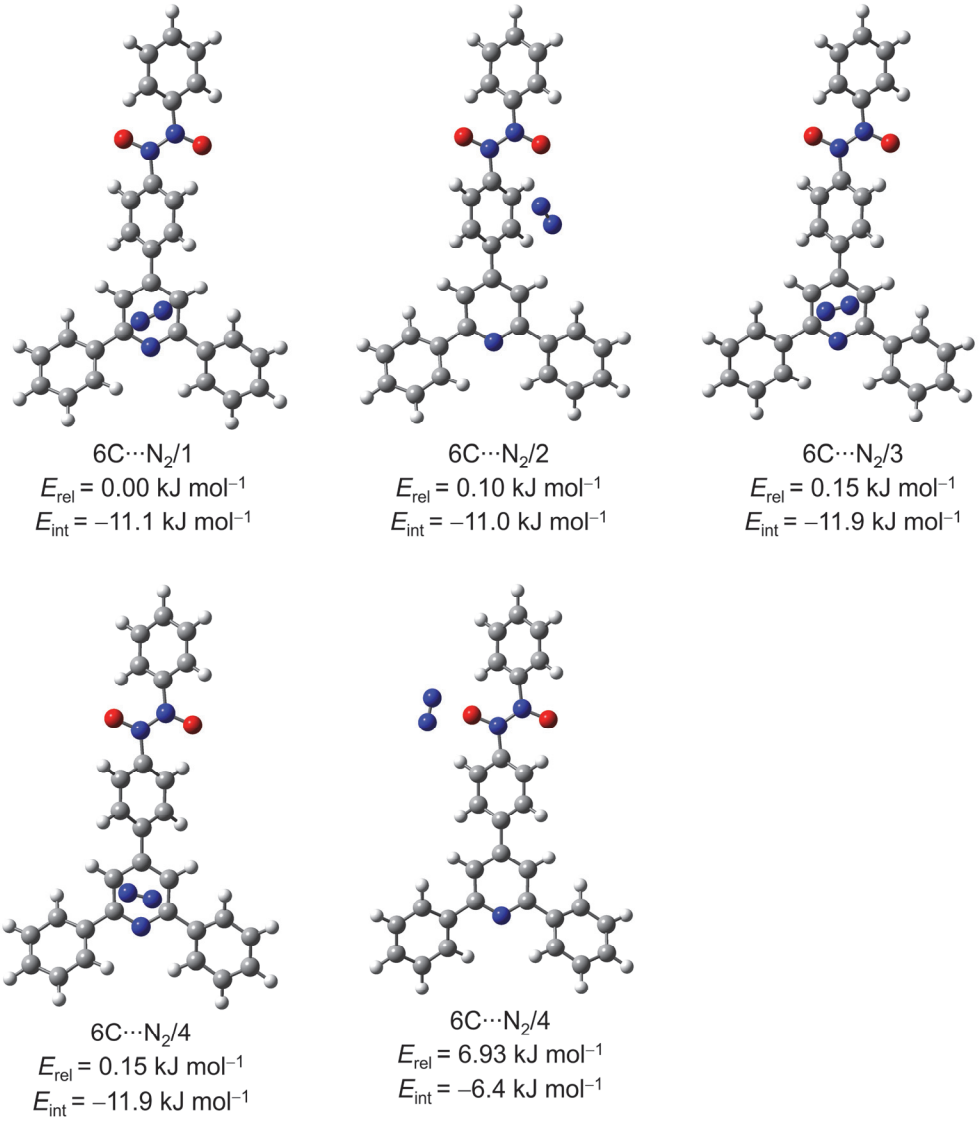

Figure S22. The B3LYP-D3(BJ)/def2-TZVP optimized geometries of the selected complexes between fragment **6C** and one molecule of N_2. Relative energies of the selected complexes (E_{rel}) and BSSE corrected interaction energies (E_{int}).

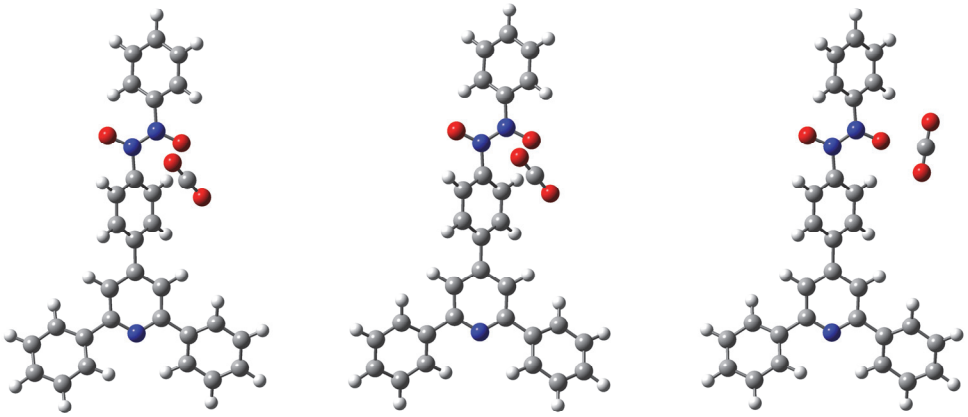

6C···CO_2/1
E_{rel} = 0.00 kJ mol^{-1}
E_{int} = –21.7 kJ mol^{-1}

6C···CO_2/2
E_{rel} = 0.39 kJ mol^{-1}
E_{int} = –21.4 kJ mol^{-1}

6C···CO_2/3
E_{rel} = 7.64 kJ mol^{-1}
E_{int} = –16.5 kJ mol^{-1}

Figure S23. The B3LYP-D3(BJ)/def2-TZVP optimized geometries of the selected complexes between fragment **6C** and one molecule of CO_2. Relative energies of the selected complexes (E_{rel}) and BSSE corrected interaction energies (E_{int}).

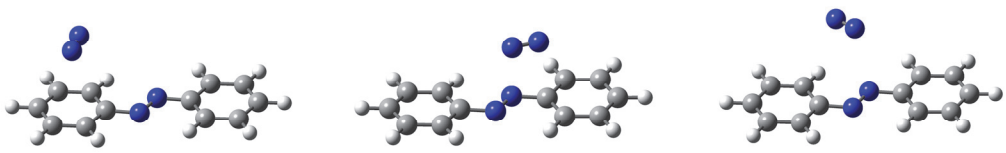

D_{azo}···N_2/1
E_{rel} = 0.00 kJ mol^{-1}
E_{int} = –7.6 kJ mol^{-1}

D_{azo}···N_2/2
E_{rel} = 0.59 kJ mol^{-1}
E_{int} = –7.0 kJ mol^{-1}

D_{azo}···N_2/3
E_{rel} = 0.65 kJ mol^{-1}
E_{int} = –6.9 kJ mol^{-1}

Figure S24. The B3LYP-D3(BJ)/def2-TZVP optimized geometries of the selected complexes between fragment $\mathbf{D_{azo}}$ and one molecule of N_2. Relative energies of the selected complexes (E_{rel}) and BSSE corrected interaction energies (E_{int}).

$D_{azo}\cdots CO_2/1$
E_{rel} = 0.00 kJ mol^{-1}
E_{int} = –16.5 kJ mol^{-1}

$D_{azo}\cdots CO_2/2$
E_{rel} = 4.52 kJ mol^{-1}
E_{int} = –11.5 kJ mol^{-1}

Figure S25. The B3LYP-D3(BJ)/def2-TZVP optimized geometries of the selected complexes between fragment **D_{azo}** and one molecule of CO_2. Relative energies of the selected complexes (E_{rel}) and BSSE corrected interaction energies (E_{int}).

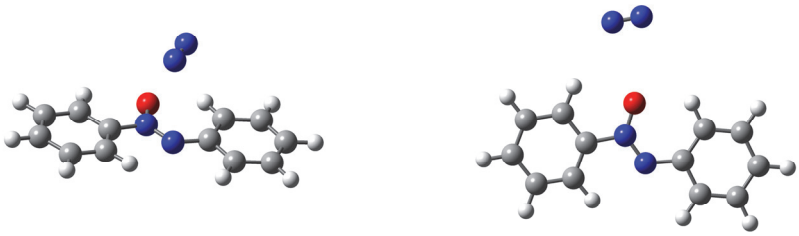

$D_{azoxy}\cdots N_2/1$
E_{rel} = 0.00 kJ mol^{-1}
E_{int} = –8.3 kJ mol^{-1}

$D_{azoxy}\cdots N_2/2$
E_{rel} = 3.28 kJ mol^{-1}
E_{int} = –5.48 kJ mol^{-1}

Figure S26. The B3LYP-D3(BJ)/def2-TZVP optimized geometries of the selected complexes between fragment **D_{azoxy}** and one molecule of N_2. Relative energies of the selected complexes (E_{rel}) and BSSE corrected interaction energies (E_{int}).

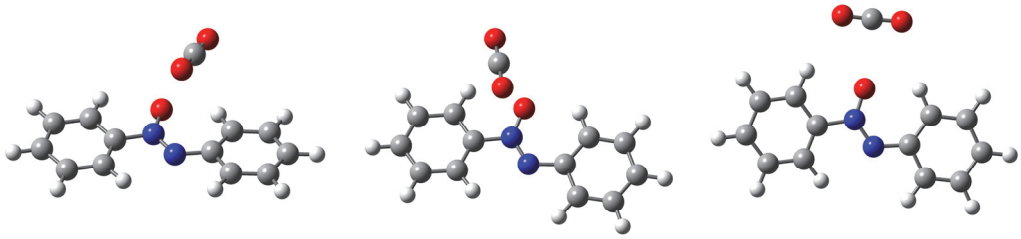

$D_{azoxy}\cdots CO_2/1$
E_{rel} = 0.00 kJ mol^{-1}
E_{int} = –17.7 kJ mol^{-1}

$D_{azoxy}\cdots CO_2/2$
E_{rel} = 1.86 kJ mol^{-1}
E_{int} = –15.7 kJ mol^{-1}

$D_{azoxy}\cdots CO_2/3$
E_{rel} = 2.75 kJ mol^{-1}
E_{int} = –15.1 kJ mol^{-1}

Figure S27. The B3LYP-D3(BJ)/def2-TZVP optimized geometries of the selected complexes between fragment **D_{azoxy}** and one molecule of CO_2. Relative energies of the selected complexes (E_{rel}) and BSSE corrected interaction energies (E_{int}).

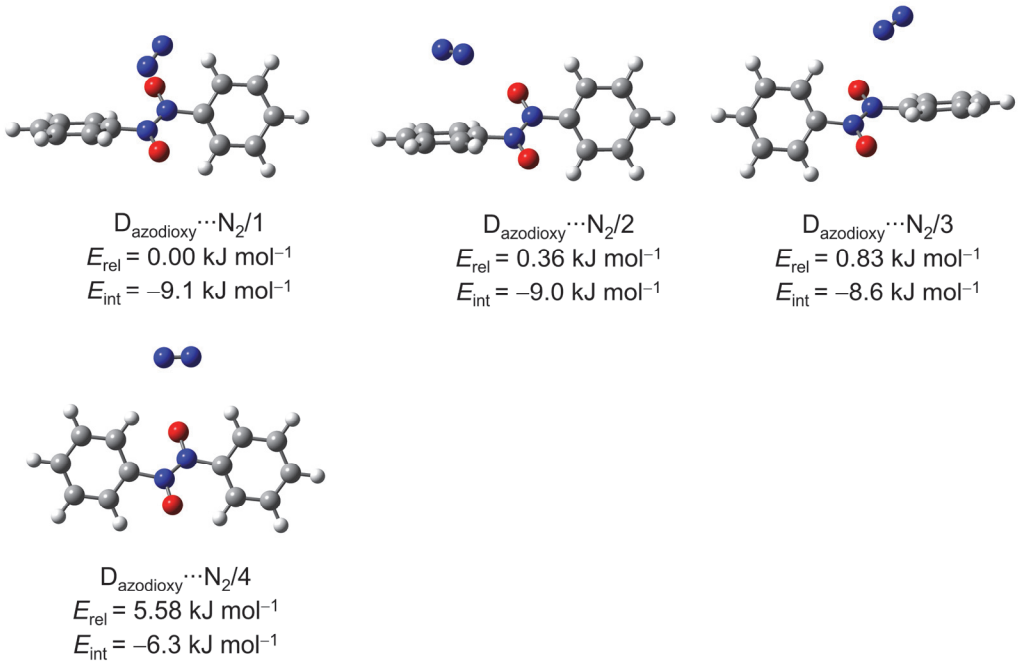

Figure S28. The B3LYP-D3(BJ)/def2-TZVP optimized geometries of the selected complexes between fragment **$D_{azodioxy}$** and one molecule of N_2. Relative energies of the selected complexes (E_{rel}) and BSSE corrected interaction energies (E_{int}).

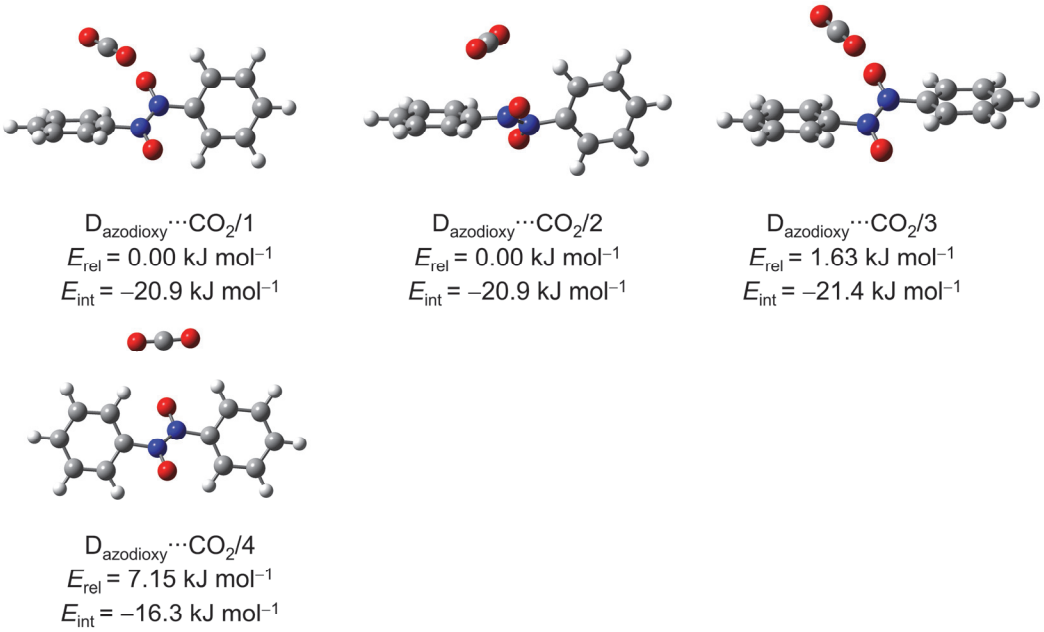

Figure S29. The B3LYP-D3(BJ)/def2-TZVP optimized geometries of the selected complexes between fragment **$D_{azodioxy}$** and one molecule of CO_2. Relative energies of the selected complexes (E_{rel}) and BSSE corrected interaction energies (E_{int}).

Table S1. Natural energy decomposition analysis (NEDA, energy contributions in kj mol^{-1}) of the selected complexes with N_2 and CO_2.

	1C···N_2	**3C···N_2**	**4C···N_2**	**6C···N_2**	**1C···CO_2**	**3C···CO_2**	**4C···CO_2**	**6C···CO_2**
Δ*E*	−10.25	−11.86	−11.17	−11.14	−17.23	−25.34	−22.78	−21.75
EL	−16.65	−19.82	−17.59	−17.48	−32.39	−44.74	−42.95	−40.85
CT	−19.58	−20.41	−22.90	−22.81	−19.85	−24.22	−21.69	−20.79
CORE	25.97	28.38	29.33	29.15	35.01	43.62	41.86	39.89
ES	−6.82	−8.37	−5.72	−5.67	−17.71	−24.46	−22.43	−21.96
POL	−19.64	−22.89	−23.74	−23.63	−29.30	−40.58	−41.04	−37.77
XC	−26.12	−28.60	−29.76	−29.70	−33.89	−46.22	−43.48	−41.53
SE1	2.09	2.97	1.73	1.73	3.78	5.98	5.93	5.30
SE2	7.72	8.46	10.13	10.08	10.84	14.32	14.58	13.59
DEF1	15.61	20.04	13.88	13.84	34.48	43.14	38.93	39.97
DEF2	46.30	48.37	57.07	56.83	49.04	67.02	66.94	60.35
POL+SE	−9.83	−11.45	−11.87	−11.82	−14.68	−20.27	−20.53	−18.89

2. Model geometries of 2D layered structures

Table S2. Unit cell parameters (*a*, *b*, *c*, α, β and γ) of the optimised geometries of compounds **1**−**6** modelled as isolated 2D layers, AA, slipped AA' and AB stacked structures. The labels of the layer group and space groups used in the CRYSTAL17.

	Compound	Space group	CRYSTAL17 label	*a* / Å	*b* / Å	*c* / Å	α / °	β / °	γ / °
2D layers	1	*P* 3*	65	20.6105	20.6105				120
	2	*P* 3*	65	20.7126	20.7126				120
	3	*P* 3*	65	21.0133	21.0133				120
	4	*P* 1*	1	26.0279	26.1225				123.5
	5	*P* 1*	1	26.3216	25.9899				123.1
	6	*P* 1*	1	26.4277	26.4674				123.5
AA	1_{AA}	$P\bar{3}$	147	20.6340	20.6340	3.8350	90	90	120
	2_{AA}	*P* 3	143	20.7754	20.7754	3.8074	90	90	120
	3_{AA}	$P\bar{3}$	147	20.9216	20.9216	3.7374	90	90	120
	4_{AA}	$P\bar{1}$	2	25.8345	26.1224	3.5616	83.2	83.7	123.1
	5_{AA}	*P* 1	1	26.4096	25.4401	3.6050	87.7	67.2	122.7
	6_{AA}	$P\bar{1}$	2	26.2274	26.2238	3.5321	93.9	94.7	123
AA' (inclined)	1_{incl}	$P\bar{1}$	2	18.9442	10.7545	6.4863	108.9	111.4	83.9
	3_{incl}	$P\bar{1}$	2	15.3047	11.0538	7.2819	111.7	48.3	108.4
	4_{incl}	$P\bar{1}$	2	25.0409	25.6254	7.7386	136.4	33.2	124.8
	5_{incl}	$P\bar{1}$	2	24.8446	25.2093	6.9099	134.8	36.8	124.1
	6_{incl}	$P\bar{1}$	2	25.4338	25.8517	7.0414	135.0	38.9	124.2
AA' (serrated)	1_{serr}	$P\bar{1}$	2	20.5117	20.6276	8.0509	106.8	81.9	119.7
	3_{serr}	$P\bar{1}$	2	20.9938	20.8784	7.8142	104.5	85.0	119.7
	4_{serr}	$P\bar{1}$	2	26.0300	22.7862	6.8638	95.5	80.3	116.4
AB	1_{AB}	$P\bar{3}$	147	20.6388	20.6388	7.2802	90	90	120
	2_{AB}	*P* 3	143	20.7754	20.7754	7.3696	90	90	120
	3_{AB}	$P\bar{3}$	147	20.9130	20.9130	7.1398	90	90	120
	4_{AB}	$P\bar{1}$	2	25.9475	23.7163	6.0332	88.0	93.4	118.8

* The corresponding layer group number, according to the International Tables for Crystallography.

Table S3. Relative energies of the optimised geometries scaled on the same number of atoms. Energies are reported relative to the energies of the **AA** configurations for each compound **1**−**6** individually.

Compound	Space group	Stacking mode	Number of atoms	E / kJ mol^{-1}
1$_{AA}$	$P\,\bar{3}$	AA	68	0.00
1$_{AB}$	$P\,\bar{3}$	AB	136	64.32
1$_{serr}$	$P\,\bar{1}$	AA' – serrated	136	0.96
1$_{incl}$	$P\,\bar{1}$	AA' – inclined	68	57.99
2$_{AA}$	$P\,3$	AA	71	0.00
2$_{AB}$	$P\,3$	AB	142	83.06
3$_{AA}$	$P\,\bar{3}$	AA	74	0.00
3$_{AB}$	$P\,\bar{3}$	AB	148	99.04
3$_{serr}$	$P\,\bar{1}$	AA' – serrated	148	12.50
3$_{incl}$	$P\,\bar{1}$	AA' – inclined	74	12.19
4$_{AA}$	$P\,\bar{1}$	AA	82	0.00
4$_{AB}$	$P\,\bar{1}$	AB	164	127.50
4$_{incl}$	$P\,\bar{1}$	AA' – inclined	164	−2.85
4$_{serr}$	$P\,\bar{1}$	AA' – serrated	164	−6.27
5$_{AA}$	$P\,1$	AA	85	0.00
5$_{incl}$	$P\,\bar{1}$	AA' – inclined	170	−4.76
6$_{AA}$	$P\,\bar{1}$	AA	88	0.00
6$_{incl}$	$P\,\bar{1}$	AA' – inclined	176	4.94

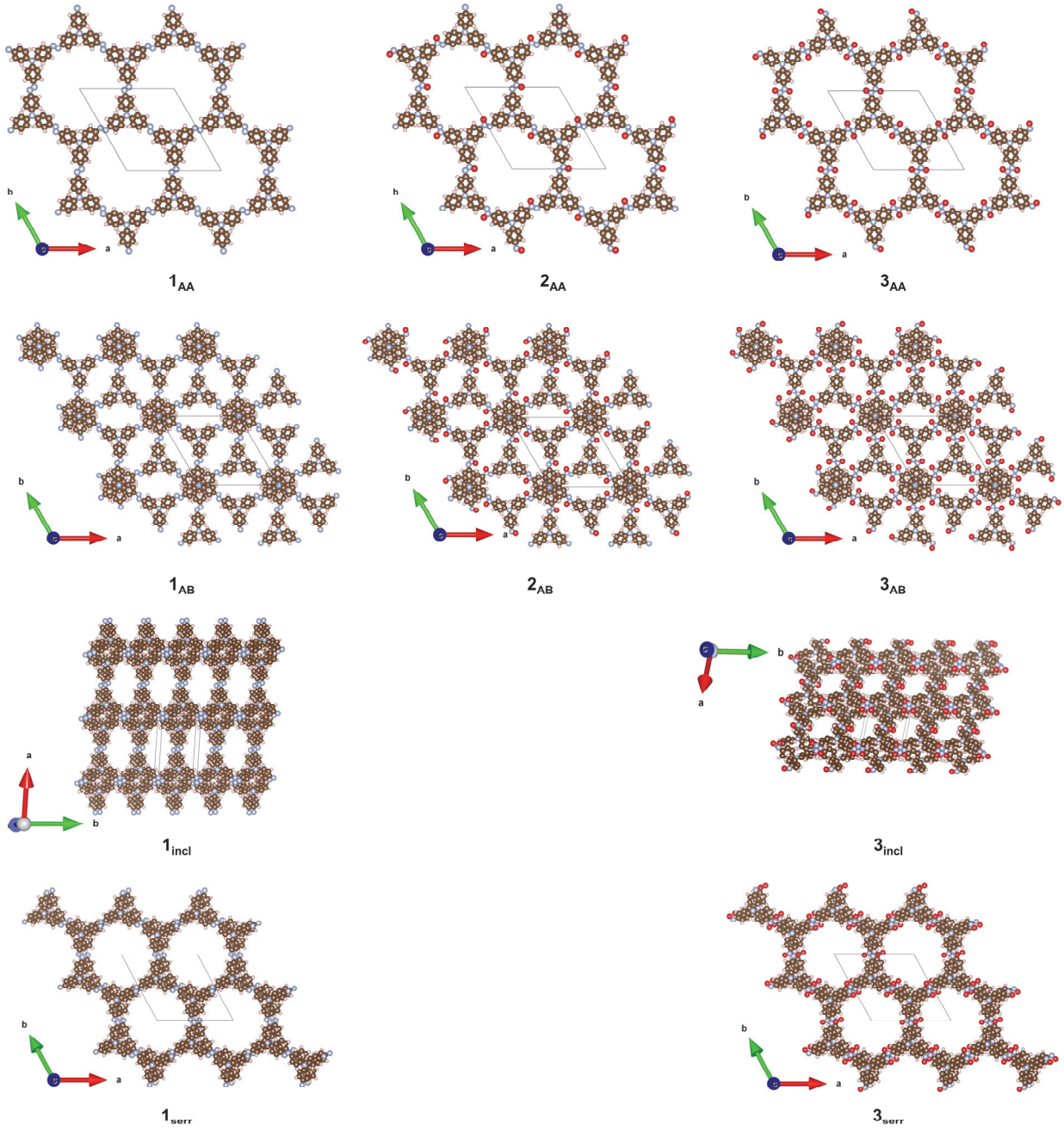

Figure S30. Schematic representation of different stacking modes of amine derivatives (TPA). Optimization was performed at the PBE-D3/pob-TZVP-rev2 level of theory.

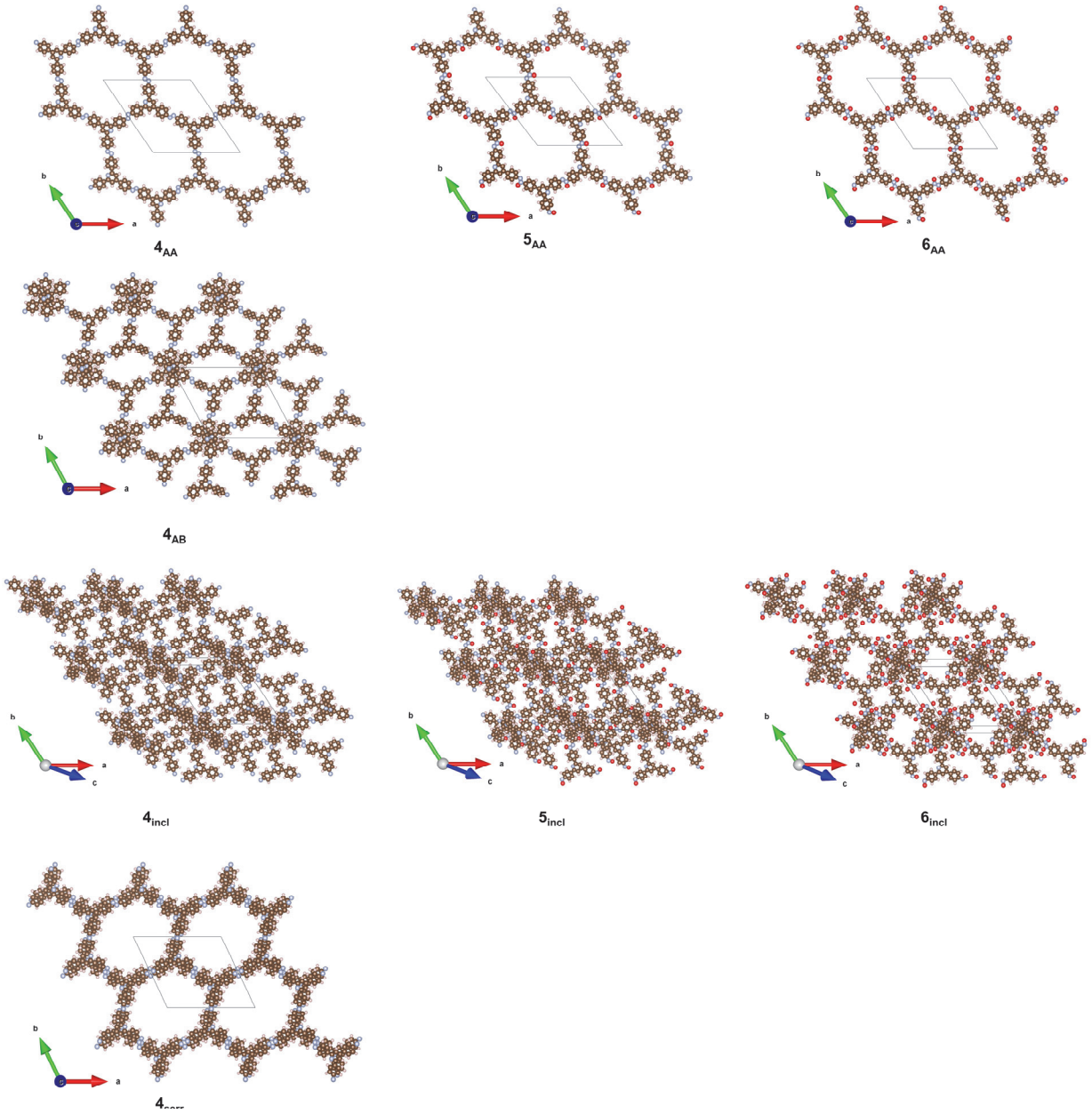

Figure S31. Schematic representation of different stacking modes of pyridine derivatives (TPP). Optimization was performed at the PBE-D3/pob-TZVP-rev2 level of theory.

3. Electrostatic potential

Table S4. Electrostatic potential values (ESP) of the most negative and the most positive regions of the selected systems **1**−**6** optimized at the PBE-D3/pob-TZVP-rev2 level of theory.

Compound	*E* / kJ mol^{-1}	Stacking mode	N	O	H	N(Py)
1$_{2D}$			−107		101	
1$_{AA}$	0.00	AA	−104 (−120)		116	
1$_{AB}$	64.32	AB	−101 −96		115	
1$_{serr}$	0.96	AA' – serrated	−96(−112)		122	
1$_{incl}$	57.99	AA' – inclined	−87 −126		128	
2$_{2D}$	0.00	AA	−73	−116	122	
2$_{AA}$	0.00	AA	−64(−69)	−127(−90)	146	
2$_{AB}$	83.06	AB	−64 −57	−130 −118	133	
3$_{2D}$				−131	114	
3$_{AA}$	0.00	AA		−110(−64)	143	
3$_{AB}$	99.04	AB		−137 −129	122	
3$_{serr}$	12.50	AA' – serrated		−109(−102)	151	
3$_{incl}$	12.19	AA' – inclined		−87 −132	129	
4$_{2D}$			−78		133	−96
4$_{AA}$	0.00	AA	−76 (−93)		144	−128
4$_{AB}$	127.50	AB	−103 −98		140	−94
4$_{serr}$	−6.27	AA' – serrated	−114(−141)		144	−136
4$_{incl}$	−2.85	AA' – inclined	−96 −69		153	
5$_{2D}$			−55	−91	142	−94
5$_{AA}$	0.00	AA	−40(−48)	−85(−113)	163	−102
5$_{incl}$	−4.76	AA' – inclined	−72	−98	156	
6$_{2D}$				−110	143	−84
6$_{AA}$	0.00	AA		−83(−63)	166	−100
6$_{incl}$	4.94	AA' – inclined		−123 −94	136 115	

4. Adsorption isotherms and density plots

Table S5. Calculated framework properties of the AA, AA' slipped and AB stacked 2D layered compounds **1**−**6** (framework density, available pore volume and nitrogen surface area). The size of the simulation box used in the GCMC calculations.

	Compound	GCMC simulation box	Framework density, g/cm^3	Available pore volume, cm^3/g	Average surface area, m^2/g
AA	1_{AA}	2×2×8	0.667	0.884	1858
	2_{AA}	2×2×8	0.720	0.805	1686
	3_{AA}	2×2×8	0.779	0.728	1501
	4_{AA}	2×2×8	0.589	1.063	1880
	5_{AA}	2×2×8	0.692	0.827	1588
	6_{AA}	2×2×8	0.651	0.959	1636
AA' (inclined)	1_{incl}	2×2×8	0.811	0.518	1395
	3_{incl}	2×2×8	1.141	0.303	742
	4_{incl}	2×2×8	1.234	0.104	132
	5_{incl}	2×2×8	1.339	0.084	194
	6_{incl}	2×2×8	1.276	0.169	342
AA' (serrated)	1_{serr}	2×2×8	0.667	0.867	1911
	3_{serr}	2×2×8	0.768	0.722	1591
	4_{serr}	2×2×8	0.638	0.917	1783
AB	1_{AB}	2×2×8	0.703	0.781	2327
	2_{AB}	2×2×8	0.743	0.734	2051
	3_{AB}	2×2×8	0.816	0.627	1570
	4_{AB}	2×2×8	0.708	0.681	1894

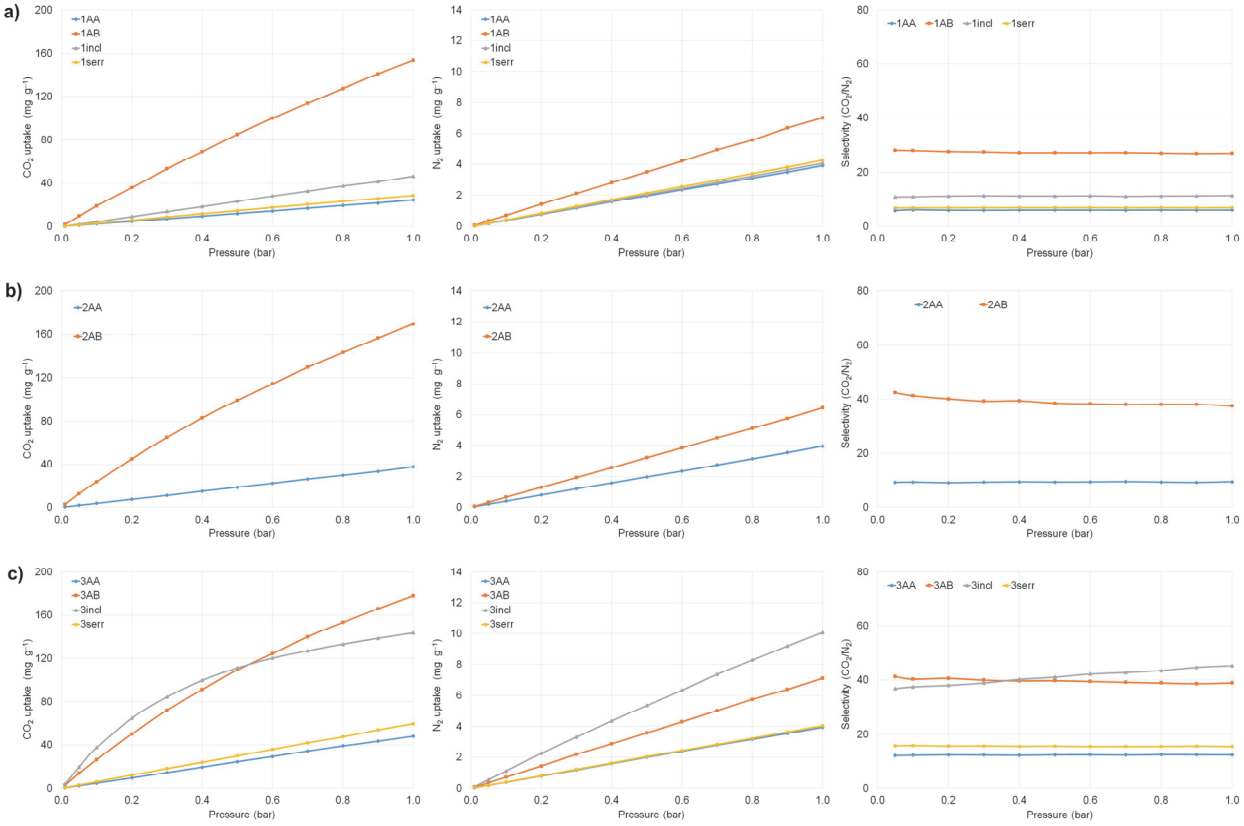

Figure S32. CO_2 and N_2 adsorption isotherms of **1**−**3** at 298 K. CO_2/N_2 selectivities of **1**−**3** for binary mixtures (15 : 85 molar ratio) at 298 K.

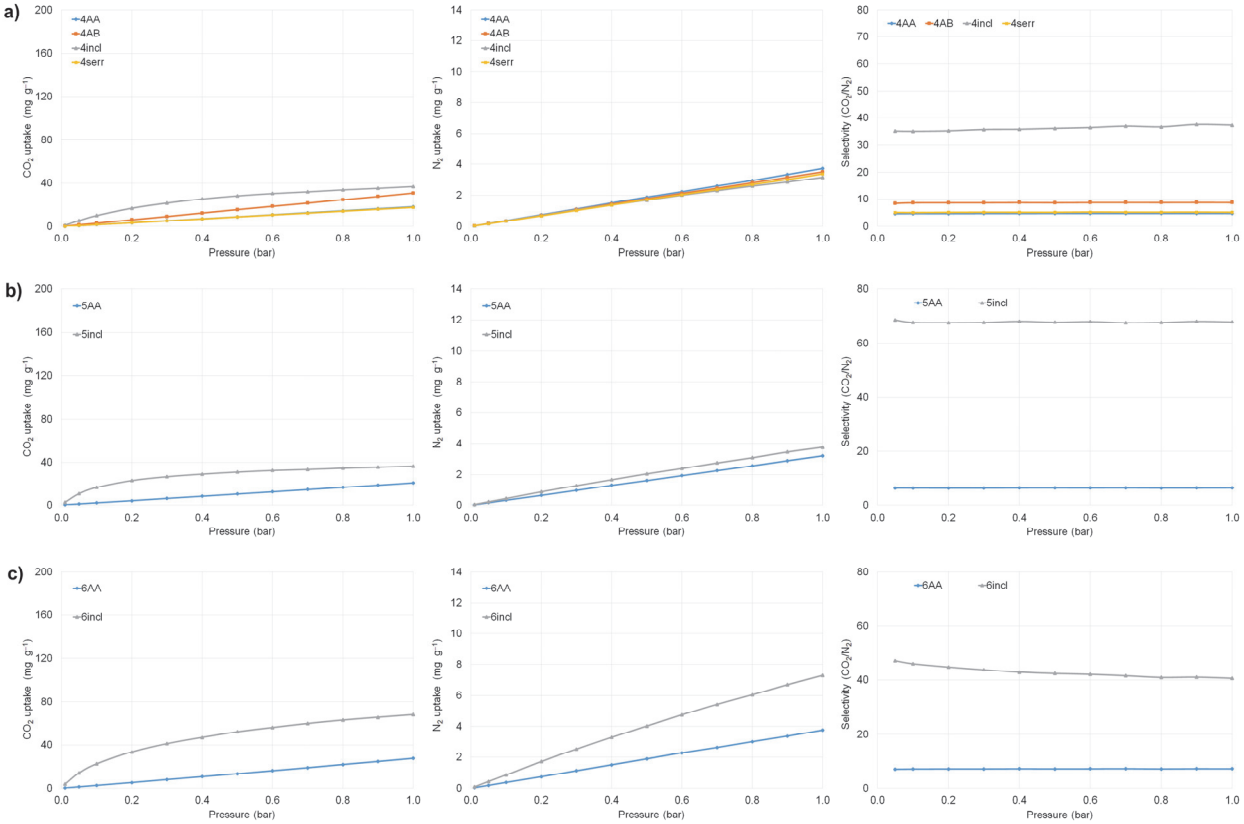

Figure S33. CO_2 and N_2 adsorption isotherms of **4**−**6** at 298 K. CO_2/N_2 selectivities of **4**−**6** for binary mixtures (15 : 85 molar ratio) at 298 K.

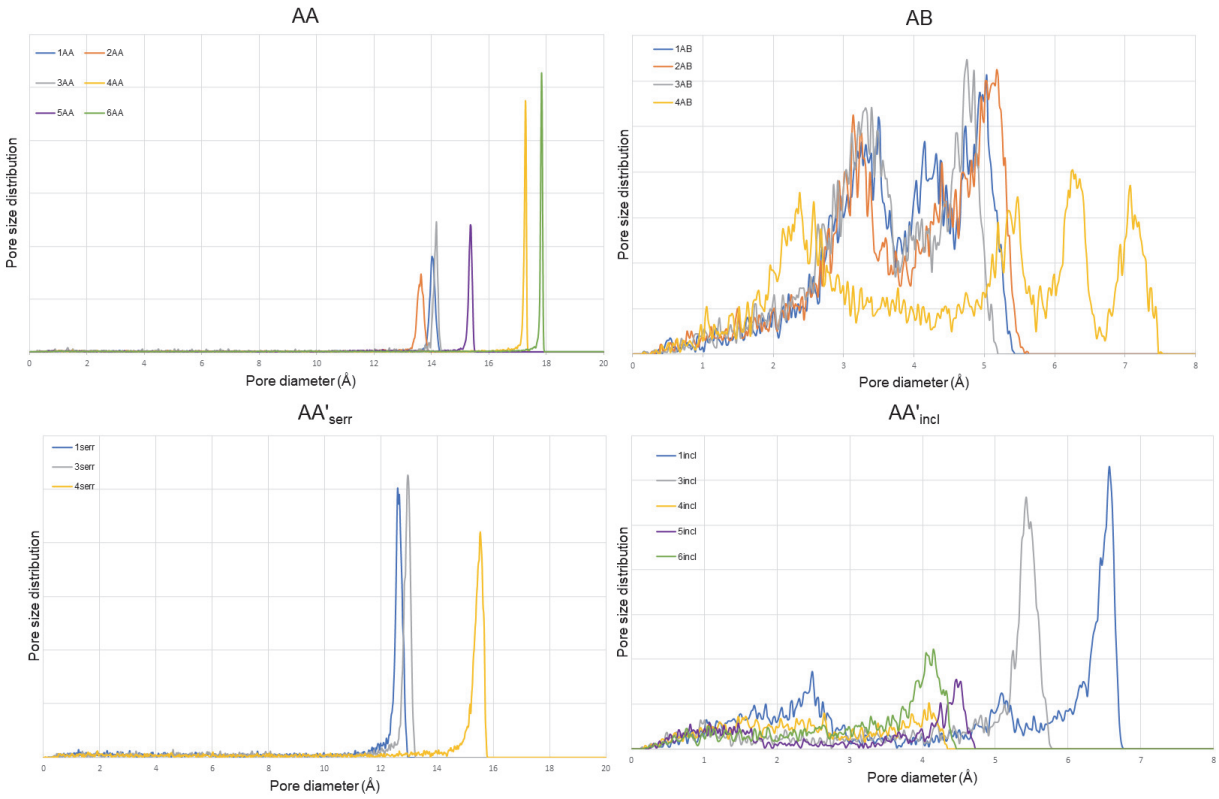

Figure S34. Pores size distribution of AA, AA' slipped and AB stacked structures of **1**−**6**.

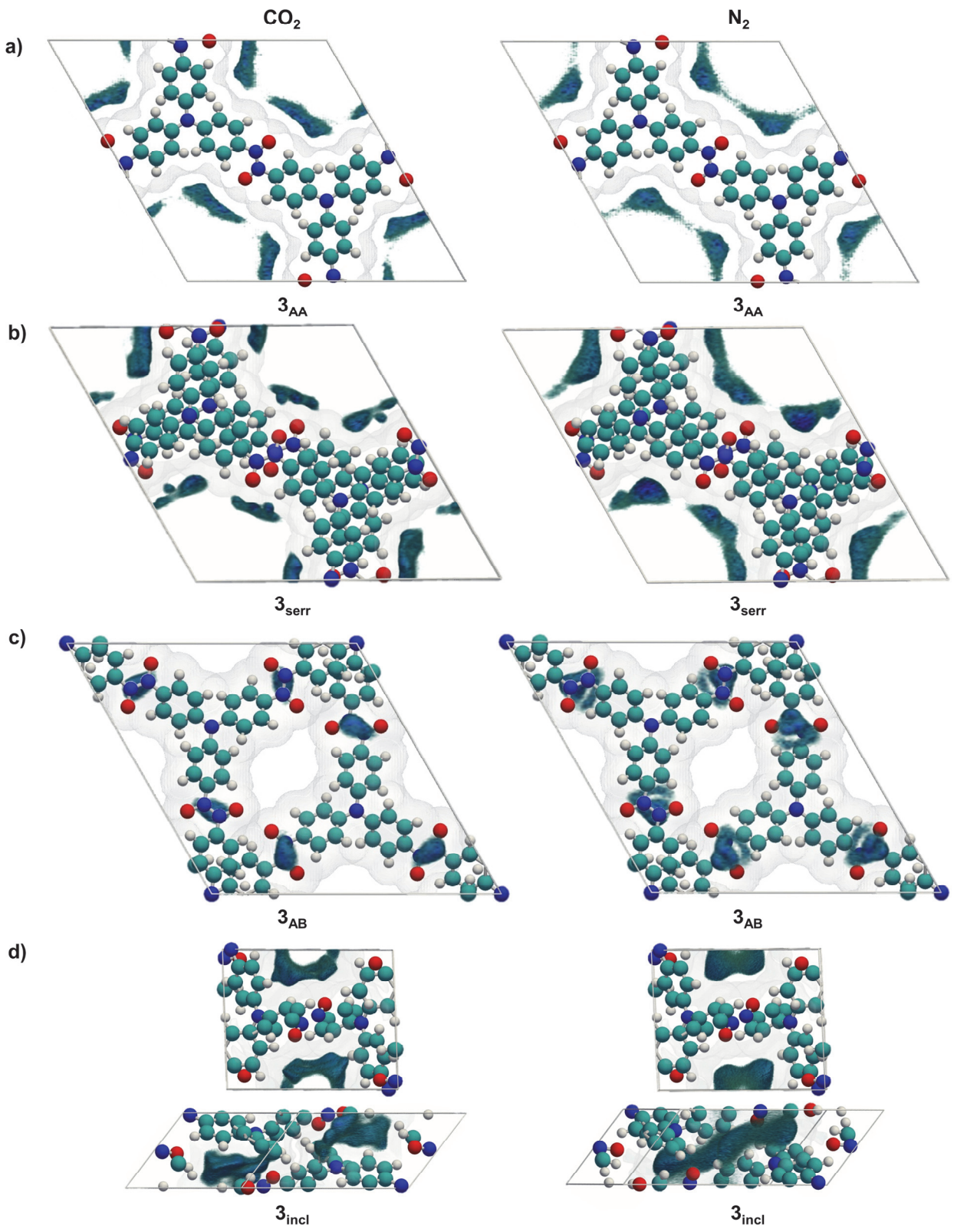

Figure S35. Density plots showing the average distribution of adsorbed N_2 and CO_2 molecules on differently stacked 2D layered frameworks of **3** at 298 K and 1 bar.

Table S6. Adsorption enthalpies (in kJ mol^{-1}) of CO_2 and N_2 with compound **3**. Van der Waals and Coulomb contributions to average host-adsorbate energies.

Compound	Average	Van der Waals	Coulomb	Van der Waals	Coulomb
$\mathbf{3_{AA}\cdots CO_2}$	−11.42	−10.86	−0.56	95%	5%
$\mathbf{3_{AB}\cdots CO_2}$	−22.75	−20.14	−2.62	88%	12%
$\mathbf{3_{incl}\cdots CO_2}$	−16.16	−14.88	−1.28	92%	8%
$\mathbf{3_{serr}\cdots CO_2}$	−12.79	−12.08	−0.70	95%	5%
$\mathbf{3_{AA}\cdots N_2}$	−5.95	−5.89	−0.07	99%	1%
$\mathbf{3_{AB}\cdots N_2}$	−10.58	−10.25	−0.33	97%	3%
$\mathbf{3_{incl}\cdots N_2}$	−8.53	−8.43	−0.10	99%	1%
$\mathbf{3_{serr}\cdots N_2}$	−6.56	−6.49	−0.07	99%	1%

Figure S36. Average host-adsorbate energies, van der Waals and Coulomb contributions to average host-adsorbate energies for interactions of CO_2 (a) and N_2 (b) with compound **3**.

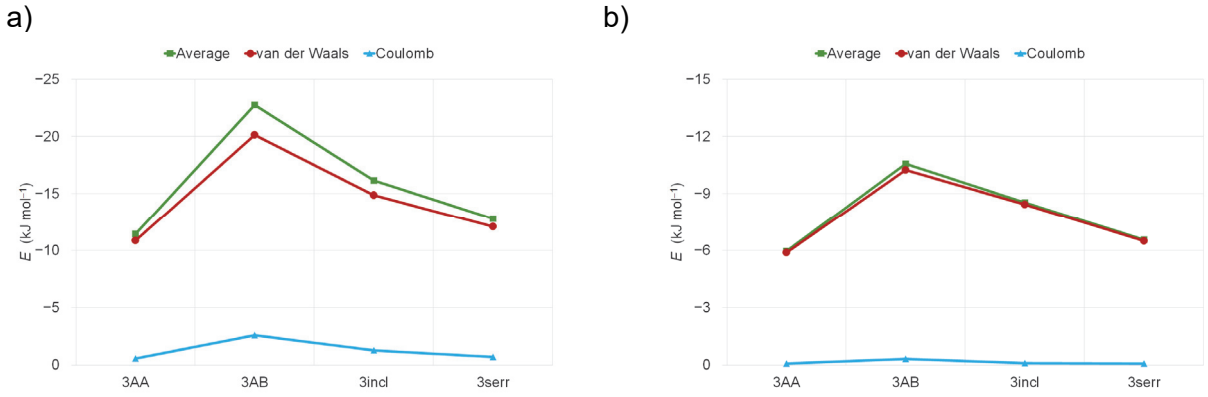

5. Correlation between the ESP values and CO_2 uptakes

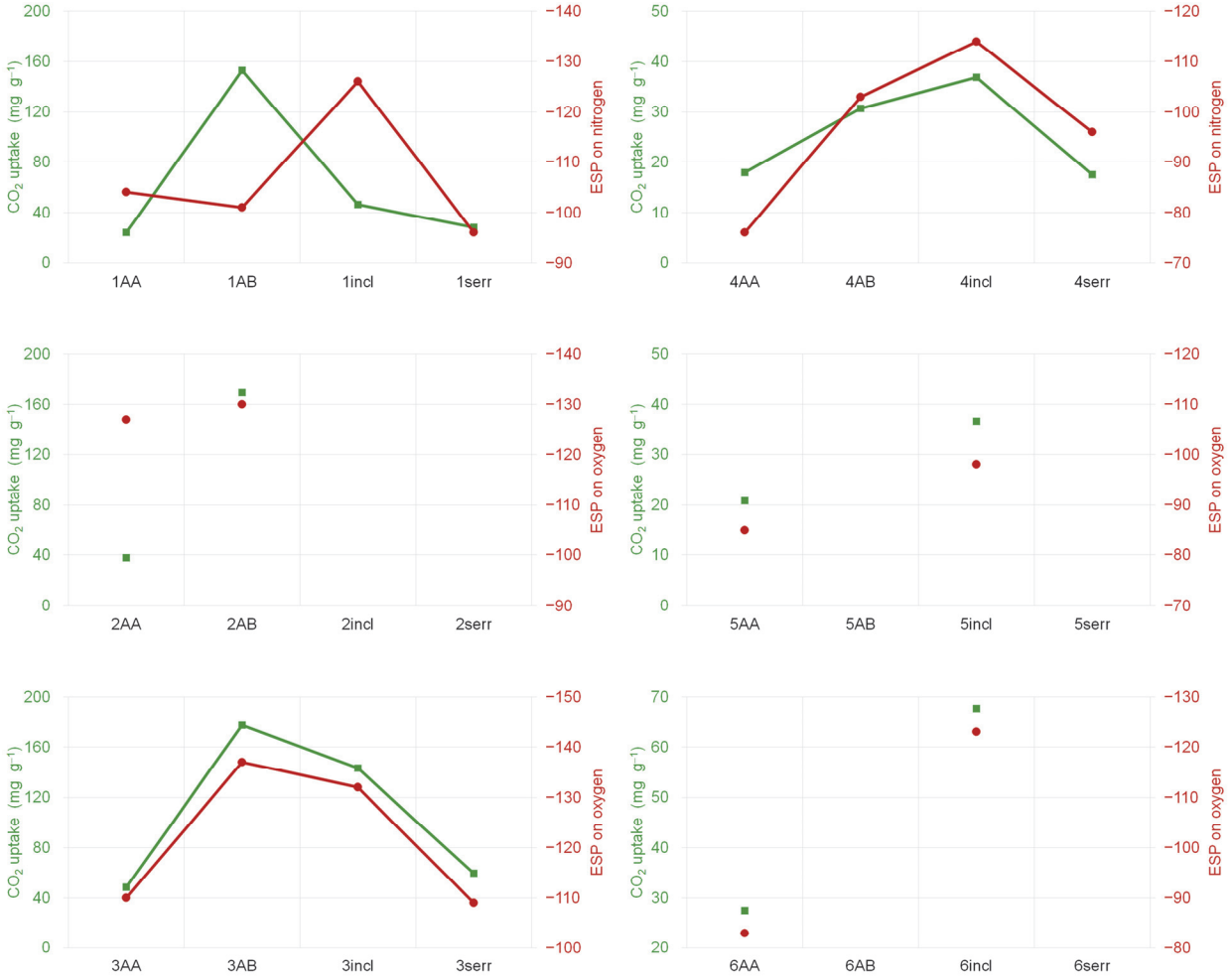

Figure S37. Correlations between the ESP values (in kJ mol^{-1} e^{-1}, reversed values on the right y-axis) calculated for the most negative regions (oxygens or nitrogens in azo, azoxy and azodioxy linakges) and CO2 uptakes (in mg g^{-1}, left y-axis) at 298 K and 1 bar calculated for different stacking modes of **1**−**6**.

6. Synthesis of 2,4,6-tris(4-aminophenyl)pyridine (TAPP)

TAPP was synthesized by the procedure described in the literature.[1]

^{1}H NMR (400 MHz, DMSO-d_6) δ / ppm: 7.97 (m, 4H), 7.68–7.66 (m, 4H), 6.70–6.66 (m, 6H), 5.44 (s, 2H), 5.37 (s, 4H).

^{13}C NMR (100 MHz, DMSO-d_6) δ / ppm: 156.7, 150.3, 150.1, 149.1, 128.0, 127.4, 125.4, 114.4, 114.0, 111.6.

IR (ATR) $\tilde{\upsilon}$ / cm^{-1}: 3401, 3299, 3203, 1594, 1540.

7. ^{13}C CP/MAS NMR spectrum of azo polymer TPP-azo (4)

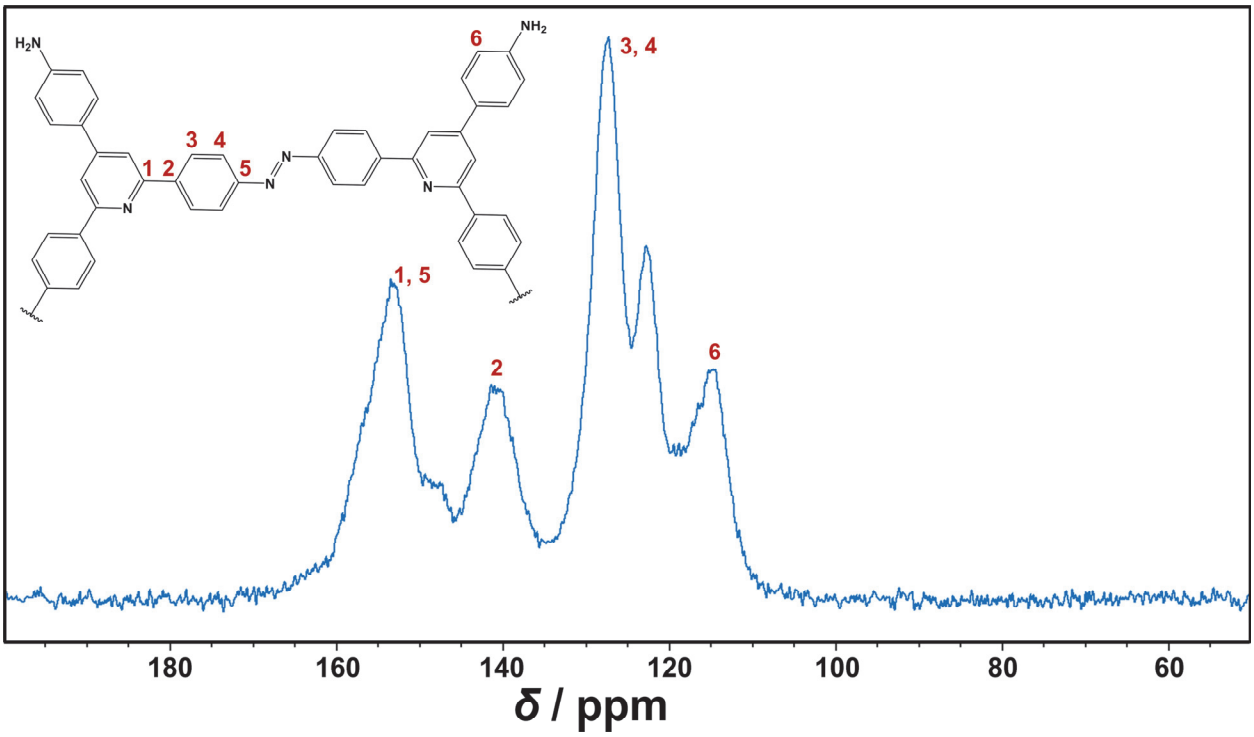

Figure S38. ^{13}C CP/MAS NMR spectrum of azo polymer TPP-azo (4).

[1] Chen, W.; Yan, W.; Wu, S.; Xu, Z.; Yeung, K. W. K.; Yi, C. Preparation and Properties of Novel Triphenylpyridine-Containing Hyperbranched Polyimides Derived from 2,4,6-Tris(4-Aminophenyl)Pyridine under Microwave Irradiation. Macromol. Chem. Phys. 2010, 211 (16), 1803–1813. https://doi.org/10.1002/macp.201000193.